Available online at www.sciencedirect.com
SCIENCE DIRECT®
International Journal of Heat and Fluid Flow 25 (2004) 499–512
International Journal of HEAT AND FLUID FLOW
www.elsevier.com/locate/ijhff

Modelling two- and three-dimensional separation from curved surfaces with anisotropy-resolving turbulence closures

C. Wang, Y.J. Jang, M.A. Leschziner *

Department of Aeronautics, Imperial College London, Prince Consort Road, South Kensington, London SW7 2AZ, UK

Abstract

The ability of non-linear eddy-viscosity and second-moment models to predict separation from two- and three-dimensional curved surfaces is examined on the basis of computations for two flows that are geometrically akin: one separating from periodically-spaced, two-dimensional 'hills' in a plane channel, and the other from a three-dimensional hill in a duct. One major objective is to examine whether the predictive performance in 3-d (three-dimensional) conditions relates to that in 2-d (two-dimensional) flow. In the former, the separation pattern is far more complicated, being characterised by multiple vortical structures associated with 'open' separation. The predicted separation behaviour in the 2-d flow differs significantly from model to model, with only one non-linear model among those examined performing well, this variant formulated to adhere to the two-component wall limit. In 3-d separation, none of the models gives a credible representation of the complex multi-vortical separation pattern.

Keywords: Separation; Curved surfaces; Turbulence modelling; Non-linear eddy-viscosity models; Reynolds-stress models

1. Introduction

Separation from curved surfaces is one of the hardest aerodynamic processes to predict correctly. Yet, it is the key to determining the gross flow properties in and the operational performance of a wide variety of engineering devices, especially in aero-mechanical engineering.

Apart from the possible existence of large scale, organised shedding-like unsteadiness, a major predictive challenge to RANS as well as LES schemes arises from the fact that even slight changes in the time-averaged location of the separation line are observed to result in substantial changes in the reattachment behaviour and thus in gross-flow features. In transonic flows, where separation is provoked by shocks, there is also a strong opposite effect of the details of the post-separation flow substantially affecting the shock and hence the separation location.

The challenges arising from unsteadiness and 'non-locality' of turbulence aside, a RANS scheme must be able to return the sensitivity of the time-mean separation process to the evolution of the boundary layer as it decelerates and skews, the latter in 3-d, while subjected to adverse pressure gradient. This is an important difference relative to separation from a sharp corner. In terms of statistical properties of turbulence, the separation behaviour depends on the differentiated response of the turbulent stresses in the boundary layer to shear, irrotational and curvature-related straining, and turbulence anisotropy is likely to play an important role in this response. Similarly complex interactions are effective in the separated, curved shear layer, in the intense streamwise vortices in 3-d flow, in the reattachment process and in the post-reattachment recovery region.

Much effort has gone in recent years into the investigation of turbulence closures more complex than linear eddy-viscosity models for separated flows, although rarely in conditions in which separation from a continuous surface is provoked by the action of a smoothly varying adverse pressure gradient. Several studies have examined the predictive performance of a range of non-linear eddy-viscosity, explicit algebraic Reynolds-stress and full second-moment models for separated laboratory flows in an effort to identify optimal modelling methodologies (e.g. Lien and Leschziner (1995, 1997), Apsley and Leschziner (1999), Hanjalic (1994), Craft (1998), May (1999), Jang et al. (2002)). Moreover, a

* Corresponding author. Tel.: +44-20-75945061; fax: +44-20-75848120.
E-mail address: mike.leschziner@imperial.ac.uk (M.A. Leschziner).

0142-727X/$ - see front matter © 2004 Elsevier Inc. All rights reserved.
doi:10.1016/j.ijheatfluidflow.2004.02.009

number of collaborative efforts, notably recent workshops organised under the auspices of ERCOFTAC (Rodi et al., 1998; Jakirlic et al., 2001, Manceau and Bonnet, 2003) have included key test cases that feature separation from curved surfaces. Most of this work has been undertaken within a 2-d framework, because of the relatively modest computational effort involved, the more abundant availability of experimental data and the promise of greater insight into fundamental issues. Although significant predictive advantages can be derived from anisotropy-resolving models in some cases, model performance has been observed to be uneven, and some of the studies involved uncertainties arising from insufficient data and 3-d contamination of the experimental flow or other experimental limitations. A crucially important open question is whether the conclusions derived for 2-d conditions translate to 3-d flows. Some encouraging indications are provided by the studies of Lien and Leschziner (1997) and Apsley and Leschziner (1999), but both involve flow-specific limitations and do not suffice to draw firm conclusions. There is, therefore, a strong need to broaden the range of 3-d flows investigated. The outcome of such investigations will, in effect, dictate whether elaborate closures will be adopted more widely for complex practical applications.

This paper focuses on two related flows featuring separation from curved surfaces, one 2-d and the other 3-d, both shown in Fig. 1. The former geometry is a nominally infinite sequence of periodic 2-d 'hills' in a channel at $Re = 21,200$, based on mean velocity and channel height. Extensive data for spanwise homogeneous and streamwise periodic flow conditions are available for this case from highly-resolved LES computations performed by Temmerman et al. (2003) on a mesh containing almost five million nodes. The 3-d geometry is a circular hill (in plan) placed on the lower wall of a duct. Its cross-section is similar in shape to that of the 2-d hill. The flow around it, at Reynolds number 130,000, based on hill height and free-stream velocity, was investigated experimentally by Simpson et al. (2002) using LDV. It features a complex, multi-vortical separation pattern in the leeward side of the hill, as shown in Fig. 9. Thus, although the 2-d and 3-d flows are geometrically akin, the latter is physically much more complex than the former.

The 2-d flow, treated as a single periodic hill-crest-to-hill-crest segment, has been the subject of a recent study by Jang et al. (2002), which examined the performance of a range of non-linear eddy-viscosity and explicit algebraic Reynolds-stress models. A particular issue addressed in that paper in relation to this flow is whether streamwise periodicity is an important aspect in judging alternative turbulence closures. Periodicity is often said to be unrepresentative of real predictive situations and assumed to pose added challenges through the fact that errors in the inner-domain solution are fed back to the inlet plane, thus progressively amplifying the departure of the model solution from reality and obscuring model capabilities. The extent to which this issue affects conclusions on closure performance and their applicability to cases in which the inlet flow is specified as a boundary condition is addressed by performing computations for

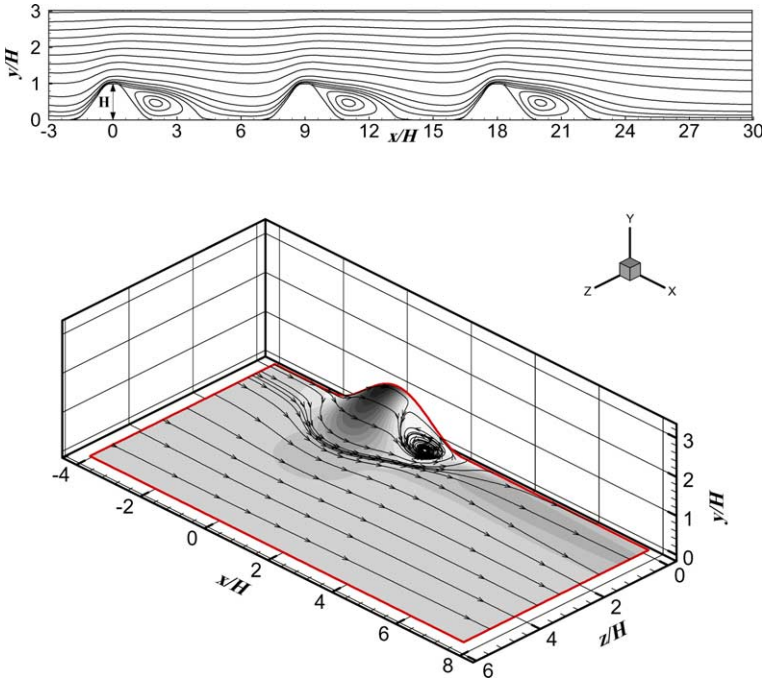

Fig. 1. Geometries investigated. Upper plot includes streamfunction contours. Lower plot contains surface streaklines.

a sequence of three hills, with LES conditions applied to the inflow plane, as well as for a single segment, with imposed periodicity conditions. The former practice allows the rate of approach to the periodic state to be studied and the 'anchoring' influence of the specified inlet conditions to be identified in terms of its importance to the assessment of turbulence models.

2. Turbulence models

Five turbulence models are investigated herein, namely: the Craft–Launder–Suga cubic eddy-viscosity model (Craft et al., 1996), the Apsley and Leschziner (1998) cubic eddy-viscosity model (AL-ε); the Wallin and Johansson (2000) explicit algebraic stress model (WJ-ω); the Abe-Jang-Leschziner quadratic eddy-viscosity model (2003) (AJL-ω); and the Speziale–Sarkar–Gatski Reynolds-stress-transport model (Speziale et al., 1991), extended to low-Re conditions by Chen et al. (2000) (SSG-ε), in which the extensions 'ε' and 'ω' to the abbreviations indicate the nature of the length-scale equation used in the models. This is a selection from a broader investigation including further non-linear eddy-viscosity and Reynolds-stress models (NLEVMs and RSTMs). The selected group contains a representative cubic model (derived from a simplified Reynolds-stress model), the most recent explicit algebraic Reynolds-stress model, (quadratic in 2-d and quadratic in 3-d), a representative Reynolds-stress-transport model and a recent quadratic model, formulated to adhere to the correct limiting behaviour of near-wall turbulence (see below). The above selection may be claimed to represent the two principal groups of anisotropy-resolving turbulence models currently considered as primary alternatives to isotropic-viscosity models for complex-flow applications. More advanced forms of second-moment closure exist (e.g. Jakirlic and Hanjalic (1995), Craft and Launder (1996), Batten et al. (1999)). However, experience suggests that their predictive performance in complex-flow conditions is not fundamentally different from that of simpler second-moment closures.

A complete mathematical description of all models is provided in Jang et al. (2002). Of these, the quadratic low-Reynolds-number model of Abe et al. (AJL-ω) is the most recent and differs in two important respects from other models of the NLEVM type. First, it augments the basic quadratic constitutive stress–strain/vorticity equation by two additive fragments intended to account, respectively, for high normal straining and strong near-wall anisotropy. Second, it uses a form of the ω-equation that is much closer than Wilcox's form to the ε-equation. Specifically, it includes products of k- and ω-gradients and coefficients for the production and destruction terms that are directly equivalent to $C_{\varepsilon 1}$ and $C_{\varepsilon 2}$ normally used in the ε-equation.

An influential model fragment accounts specifically for strong near-wall anisotropy and for the correct decay towards two-component turbulence that is observed in DNS. This decay cannot be represented solely by the use of terms combining the strain and vorticity. The approach taken by Abe et al. was thus to add a tensorially correct wall-related term to the constitutive stress–strain/vorticity relation $a_{ij} \equiv \frac{\overline{u_i u_j}}{k} - \frac{2}{3}\delta_{ij} = f(S_{ij}, \Omega_{ij} \ldots)$, which takes into account the wall orientation. In the model variant used here, the wall-direction indicator is: $d_i = N_i/\sqrt{N_k N_k}$, $N_i = \partial l_d/\partial x_i$, $l_d = y_n$ (wall distance) which is then used in the additive wall-anisotropy correction of the form:

$$
{}^{w}a_{ij} = -f_w\left(d_i d_j - \frac{\delta_{ij}}{3} d_k d_k\right) \times f(S_{ik}S_{kj}, S_{ik}\Omega_{kj}, S_{kj}\Omega_{ik}, S^2, \Omega^2 \ldots),
$$

where f_w is a viscosity-related damping function (see Jang et al. (2002) for details). Alternative wall-orientation indicators that are independent of wall distance may readily be used. In the above damping function, a composite time scale is used, which combines the macro-scale k/ε with the Kolmogorov scale $\sqrt{\nu/\varepsilon}$. The damping function f_w then provides a smooth transition between the two scales across the near-wall layer. The model is fully described in Abe et al. (2003) and Jang et al. (2002), and the latter publication demonstrates, by way of results for the anisotropy and its invariants, that the model indeed returns the correct wall-asymptotic behaviour of the stresses for the separated flow in the 2-d constricted channel also considered in this paper.

3. Computational issues

3.1. Numerical procedure

Computations were performed with a non-orthogonal, collocated, cell-centred finite-volume approach implemented in the code 'STREAM' (Lien and Leschziner (1994), Apsley and Leschziner (1999)). Convection of both mean-flow and turbulence quantities is approximated by the 'UMIST' scheme (Lien and Leschziner (1994))—a second-order TVD approximation of the QUICK scheme. Mass conservation is enforced indirectly by way of a pressure-correction algorithm. Within this scheme, the transport and the pressure-correction equations are solved sequentially and iterated to convergence.

3.2. 2-d Hill flow

Previous computations by Jang et al. (2002) have treated this flow as perfectly periodic. Here, in contrast, a sequence of three hills is considered for reasons

explained in the introduction. Inlet conditions, taken from the LES solution, were specified 2 hill heights upstream of the first hill, a position at which the flow undergoes recovery from the reattachment 2.5 hill heights further upstream. Following grid-dependence tests, in addition to those undertaken earlier by Jang et al. (2002) for the periodic segment, a non-uniform body-fitted H-type grid comprising 700×90 nodes has been used. The grid is compressed towards the walls, with five nodes covering the viscous sub-layer down to $y^+ = 0.5$. The channel following the third hill is extended to allow the flow to recover to a state permitting zero-streamwise-gradient conditions to be prescribed with little error. Although the hill-to-hill distance allows for a significant length of post-reattachment recovery, the above practice poses some (probably minor) uncertainty in terms of the influence of any downstream hill on the separated flow upstream of that hill.

3.3. 3-d Hill

The hill, having a base diameter of four heights and shape defined by Bessel functions, stands on the lower wall of a sufficiently large duct to be only subjected to the lower-wall boundary layer. The thickness of this layer, 2 hill-heights upstream of the hill, is approximately 0.5 hill heights. Measurements for this case are available, in the form of profiles of mean-flow, Reynolds-stresses and their orientation, at 3.63 hill heights downstream of the hill crest, the latter located at $x/H = z/H = 0$. In addition, hill-topology results are reported. Unfortunately, no upstream conditions are available, so that the inlet flow cannot be specified directly. Instead, profiles of velocity and Reynolds stresses have been measured in the duct *with the hill removed* at the location corresponding to the hill centreline. To generate inlet conditions, pre-cursor, hill-free duct calculations were performed over a length of 20 hills heights, and the reference hill-top conditions, as returned by the computation, were determined by matching the solution to the measured duct-flow profiles. The result of this matching process is indicated in Fig. 2 for the particular case of the AL-ε model. The conditions returned by the solution 4 hill heights upstream of the matching location were then taken as inlet conditions for the hill calculations. The sensitivity to errors in the matching process was then investigated by repeating some hill computations with inlet conditions

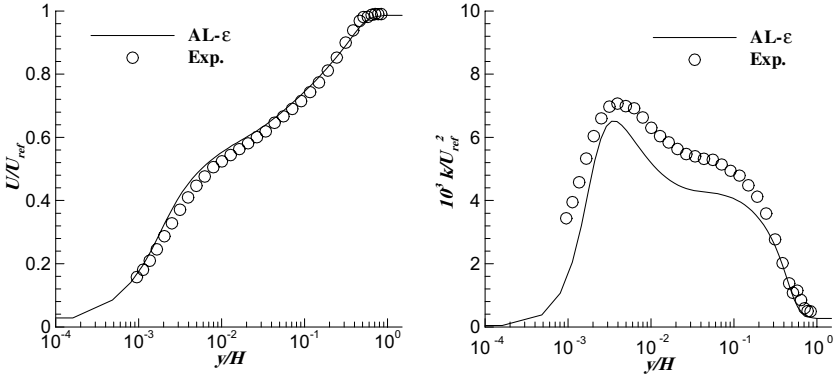

Fig. 2. 3-d Hill—matching between the calculation for the hill-free duct flow and the experimental data at $x/H = z/H = 0$ with the Apsley–Leschziner cubic eddy-viscosity model.

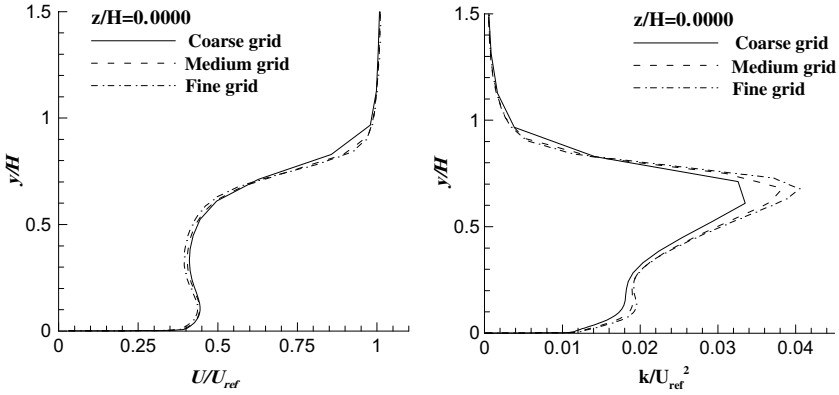

Fig. 3. 3-d Hill—grid-dependence tests with 0.3, 1.0 and 2.2 million nodes; streamwise- velocity and turbulence-energy profiles at $x/H = 3.63$.

taken at 1 hill height upstream and downstream of the reference location.

The computational domain is shown in Fig. 1 and extends over one half of duct cross-sectional area (time-accurate unsteady computations over the whole duct are commented upon below). The H-type, single-block, body-fitted grid covering the domain comprises $110\times105\times80$ (approximately one million) nodes, with the wall-nearest nodes lying within $y^+ < 1$. Grid-independence tests were conducted with three grids containing, respectively, 0.3, 1.0 and 2.2 million nodes. Fig. 3 shows profiles of streamwise velocity and turbulence energy predicted at $x/H = 3.63$ with the cubic model of Apsley and Leschziner (1998) and the three grids. Grid-dependence is seen to be minor, as it is in respect of other flow properties, and will be shown below to be wholly insignificant relative to discrepancies between all computations and the experimental data.

4. Results

4.1. 2-d Hill

It is recalled first that the principal purpose of this section is to examine the sensitivity of turbulence-model performance to the imposition of streamwise periodicity, relative to an explicit prescription of the flow-inlet conditions; a detailed interpretation of the predicted physical flow features by the various models is provided, for the periodic implementation, in the article by Jang et al. (2002).

An overall view of the predicted mean-flow characteristics, relative to the LES solution is provided in Fig. 4. This shows stream-function contours for the flow between the second and third hills, and below them, related plots showing how the reattachment location changes as the flow progresses from the first to the second and to third hill. The uppermost l.h.s. plot is the reference LES result. The hill-to-hill variation in terms of the reattachment location is compared with that returned by the periodic and LES solutions, both represented by related horizontal lines, identifying hill-independent values. Profiles of the streamwise velocity, Reynolds shear stress and turbulence energy two hill heights downstream of the hill crest, predicted by the five models outlined in Section 2, are shown in Figs. 5–7, respectively [1]. Each plot contains five profiles: one the reference LES solution, one the period solution reported by Jang et al. (2002), and three profiles relating to the conditions after the first, second and third hills, respectively.

[1] For hill segments 2 and 3, $x/H = 2$ should be interpreted as $x/H = 9 + 2$ and $18 + 2$, respectively.

Fig. 4 demonstrates the degree to which the imposition of periodicity does or does not impact on the assessment of models' predictive characteristics. It is arguable that streamwise periodicity is unrepresentative of practical problems in which the prescribed upstream conditions tend to 'anchor' the solution, so that model defects are understated, while defects are amplified by the feedback mechanism inherent in the imposition of periodicity. The present results do not support this argument. As seen, a model returning a periodic solution that is relatively far from the correct one (e.g. WJ-ω) also gives large errors in the non-periodic implementation. Indeed, for some models, the error is initially larger, with the solution eventually settling—as must be the case—towards that of the periodic implementation. The profiles in Figs. 5–7 show that, unless a model returns an especially poor representation for the periodic state, the main predictive characteristics of that model are well established after the first hill, and that only relatively minor changes in the flow structure occur as the flow progresses downstream. Self-evidently, this is especially so in the case of a model that gives a periodic solution that is close to the baseline LES field. This applies, in particular, to the Abe–Jang–Leschziner model that is shown in Jang et al. (2002) to give the best representation of the flow and also performs well in a priori tests based on the LES fields (see Jang et al. (2002)). Fig. 8, showing the skin friction on the lower wall for the periodic segment, reinforces this observation. As seen, the AJL-ω model returns, here again, the best representation over most of the wall. However, despite this generally favourable predictive quality, Figs. 6 and 7 demonstrate that even this model returns insufficient turbulence activity in the separated shear layer—a defect common to all models and probably reflecting large-scale unsteadiness in the separation location, as discussed in the introduction. Of the models examined, that by Wallin and Johansson (WJ-ω) does least well, giving a seriously excessive separation length. The SSG model, with which the WJ model is associated, performs almost as badly. Although Fig. 4 shows this model to return a broadly correct reattachment location, this is a consequence of the doubling-up of the separation streamline close to reattachment, a defect often observed in the applications of Reynolds-stress-transport models to 2-d separated flow. This masks the misrepresentation of the general structure of the recirculation region, which is evident from Fig. 4.

4.2. 3-d Hill

The principal experimental data available for this case are velocity and Reynolds-stress profiles 3.63 hill heights downstream of the hill crest. Derived from these are further data for the parameter $S^{-1} =$

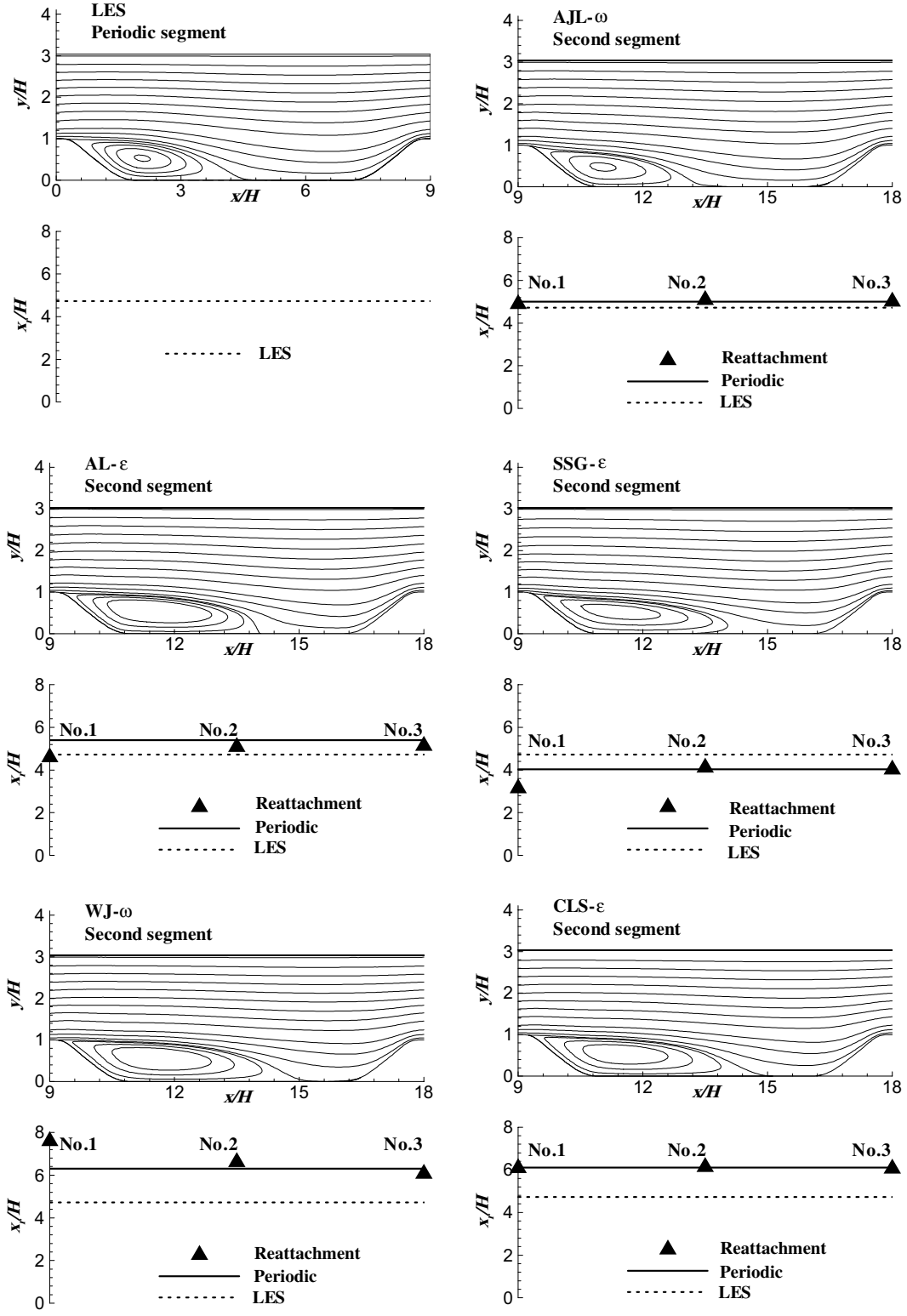

Fig. 4. 2-d Hill—stream-function contours for the second hill-to-hill segment and related plots of hill-specific reattachment locations, compared to LES solution (top l.h.s. plot).

$\sqrt{(-\overline{uv})^2 + (-\overline{vw})^2/\overline{vv}}$, which may be regarded as an anisotropy parameter. Additional surface data include oil-film traces on the hill surface, pressure and a skin-friction distributions on the hill surface.

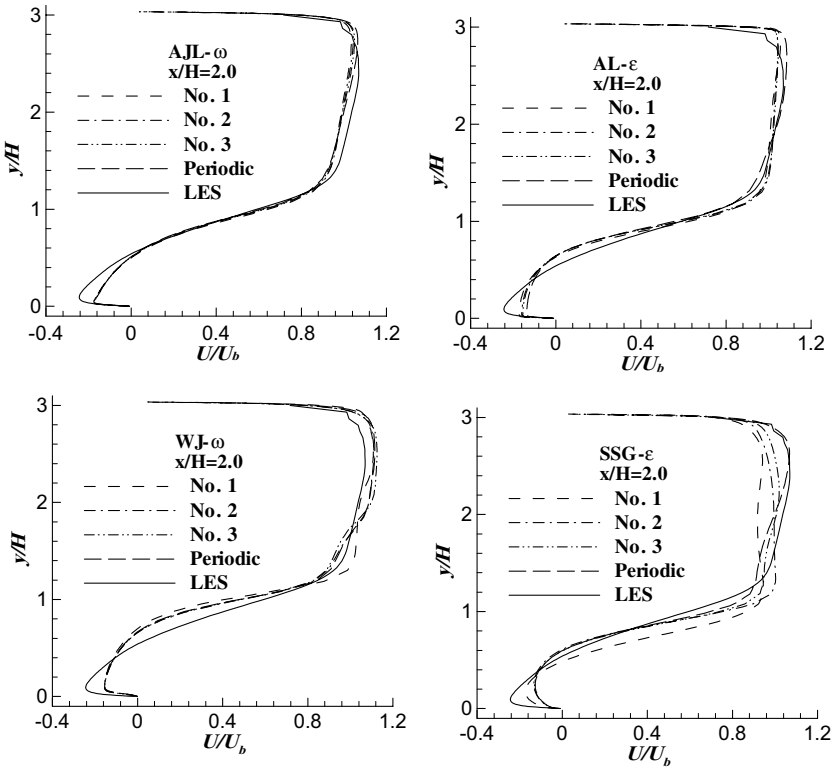

Fig. 5. 2-d Hill—profiles of streamwise velocity 2.0 hill heights downstream of relevant hill crest.

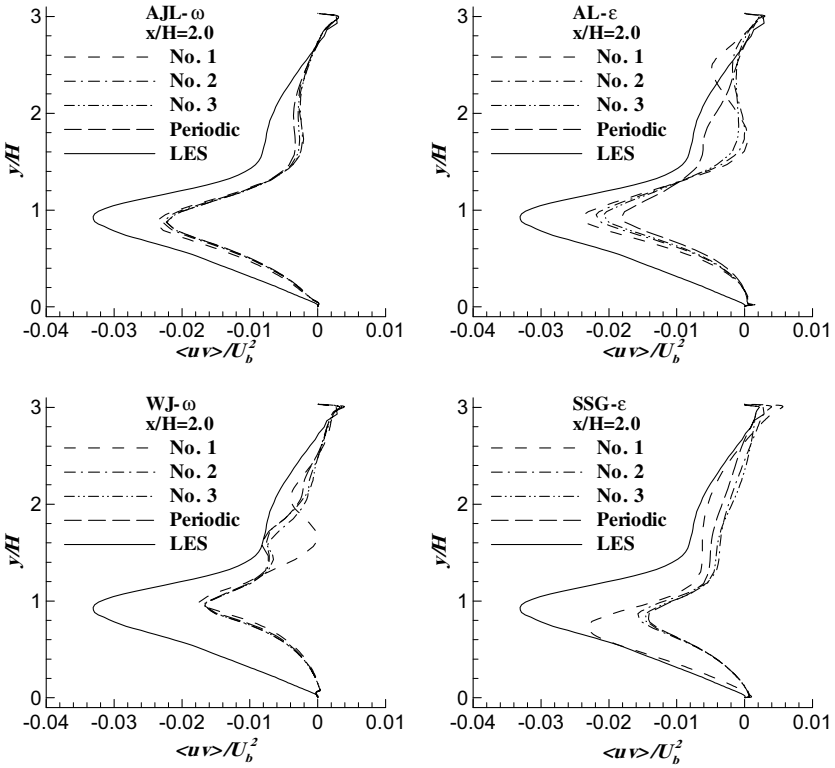

Fig. 6. 2-d Hill—profiles of the Reynolds shear stress 2.0 hill heights downstream of relevant hill crest.

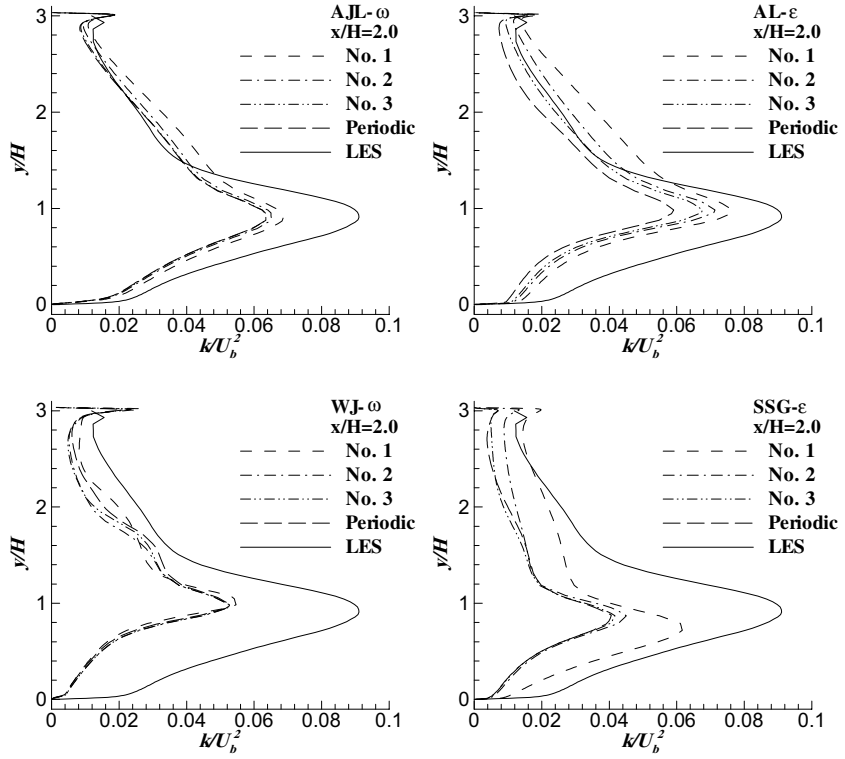

Fig. 7. 2-d Hill—profiles of the turbulence energy 2.0 hill heights downstream of relevant hill crest.

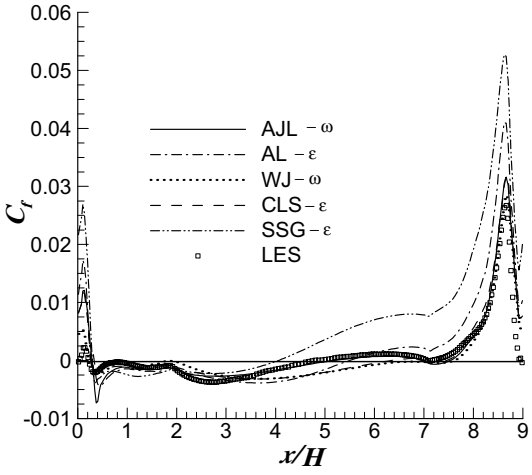

Fig. 8. 2-d Hill—distributions of skin friction on the lower (hill) wall for the periodic segment.

Fig. 9 compares predicted skin-friction (or limiting streamlines) on the hill surface with a topological map extracted from the oil-film experiments. As is evident, there are major differences between all model predictions and the experiment. The latter shows footprints of three distinct vortex pairs, while the models all predict a single pair associated with a single separation line on the hill's leeward side.

In the experiment, the vortices detach from the leeward hill surface at a relatively high elevation. Below these vortices, fluid is being drawn inwards from both sides towards the central leeward region, resulting in a downwash towards the base of the hill and creating a distinctive impingement node 'N_s' in the experimental topology map. The fluid moving downwards finally spreads outwards across the wall, feeding the detaching vortices and the wake, the latter process causing a rapid reduction in the momentum deficit in the wake and an outward spreading in the recovering wake behind the hill. Simultaneously, fluid is flowing around the base of the hill, below the vortices, towards the central leeward region. These two flow components then merge behind the hill, creating the two dashed reattachment lines.

While there are clearly subtle differences among the computational predictions, all fail to return the complex flow features described above. The strong single vortex pair in the leeward hill side extends to the base of the hill and does not permit fluid to be drawn into the base from above to feed the wake and initiate the experimentally observed rapid downstream recovery and the lateral spread of the wake. This is well brought out by the 'virtual particle' traces and transverse-velocity-vector fields shown in Fig. 10. The origins of the four traces are identical in all plots and are located slightly above the surface and slightly upstream of the hilltop. While the downstream evolution of the traces indicates not insig-

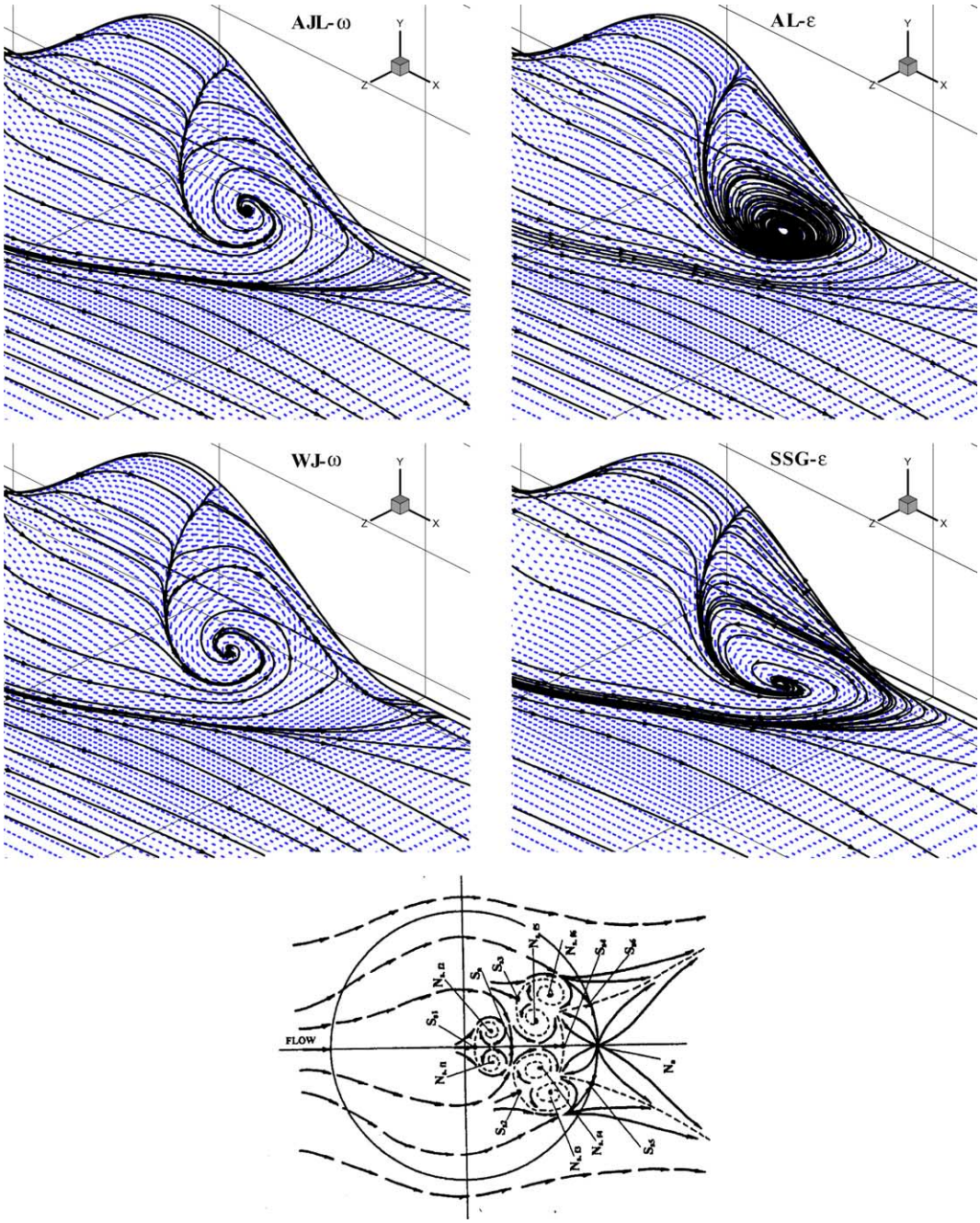

Fig. 9. 3-d Hill—predicted skin-friction lines on the hill surface in comparison with experimentally-derived topology map.

nificant differences among the predicted vortex structures, they clearly show, as do the transverse-velocity plots, that the flow close to the base of the hill is dominated by an inward motion towards the centre plane followed by an upward motion at this plane away from the lower wall.

One major consequence of the above structural differences is a much narrower and more intense wake predicted by the calculations in comparison with reality. This emerges from Fig. 11 which gives wall-normal profiles of streamwise velocity at different spanwise locations predicted with the AJL-ω and the SSG-ε models. The solutions derived from the other two models are qualitatively similar. The differences between the predictions and the experiment reflect the much more intense reverse flow predicted by all models in the leeward central portion of the hill's surface and the absence of the downwash described above. They are also consistent with the much faster experimental pressure recovery behind the hill, relative to the plateaus in the

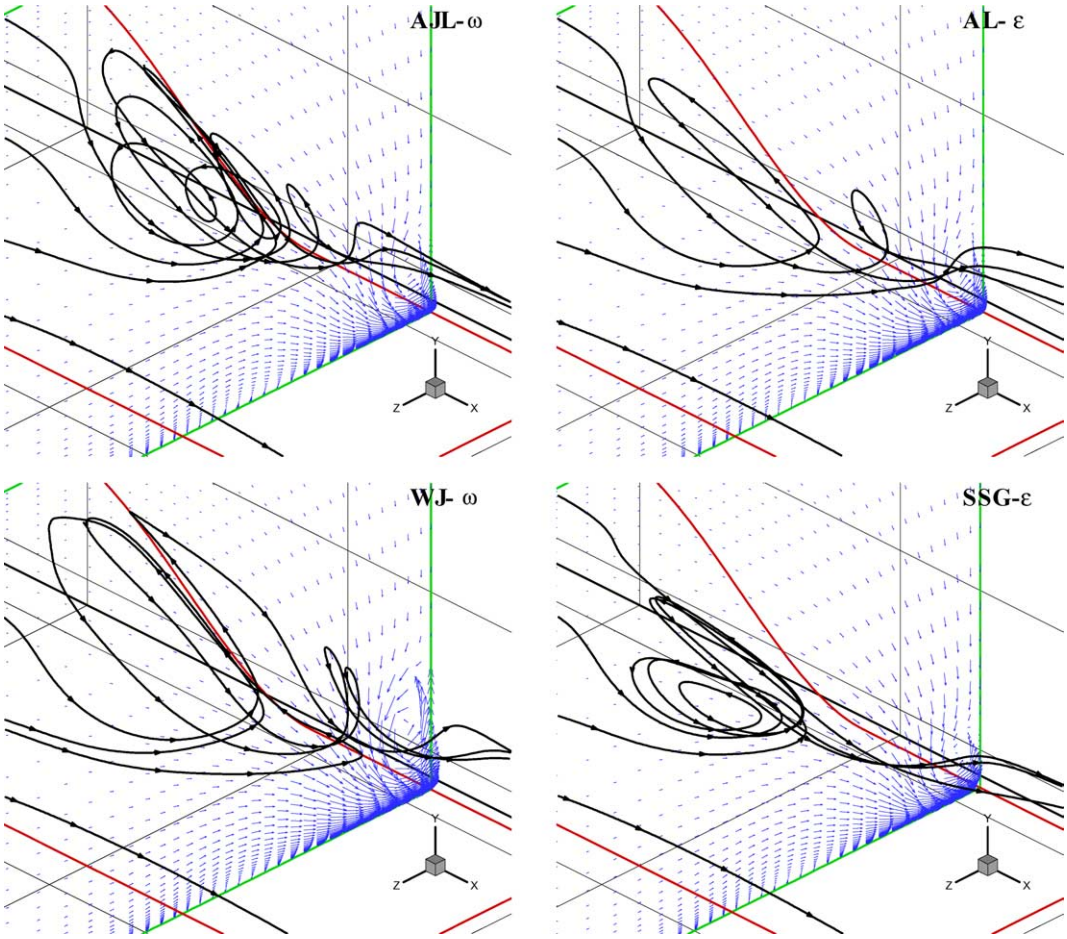

Fig. 10. 3-d Hill—virtual-particle trace lines and transverse-velocity fields at $x/H = 2.0$ illustrating the separation and vortical behaviour in the hill's leeward side.

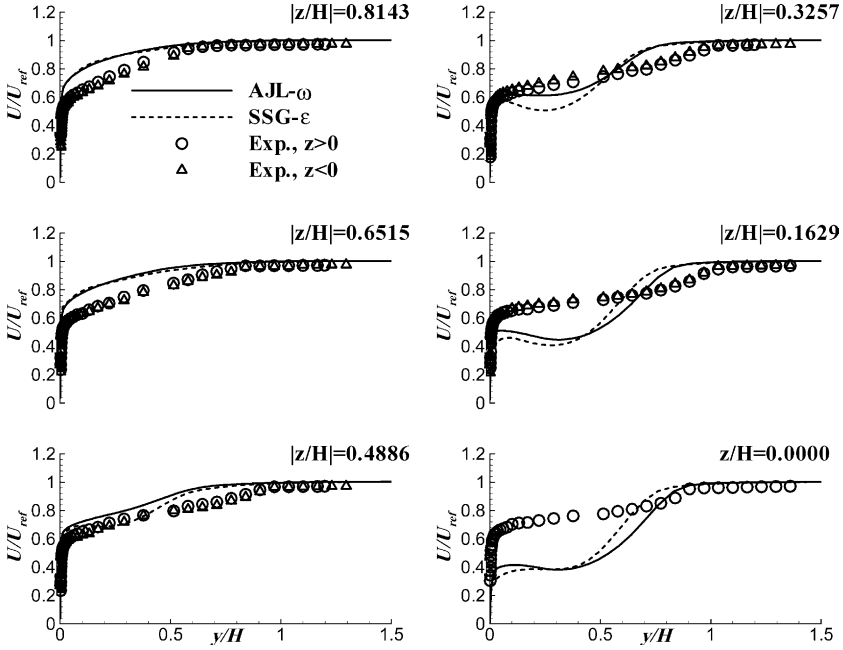

Fig. 11. 3-d Hill—profiles of streamwise velocity at $x/H = 3.63$ and various spanwise z/H locations.

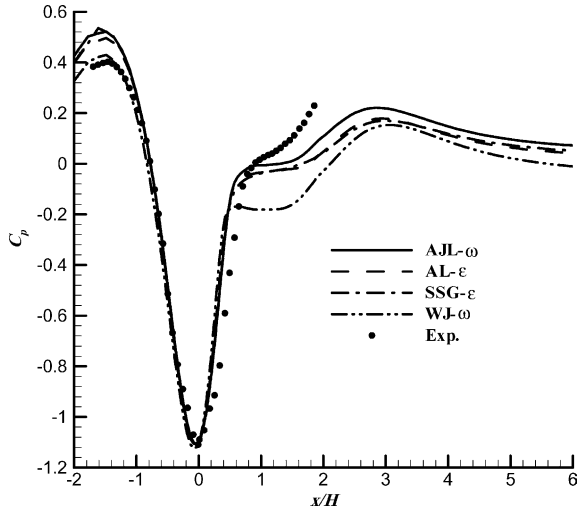

Fig. 12. 3-d Hill—distributions of pressure coefficient on the hill wall along the spanwise mid-plane $z/H = 0$.

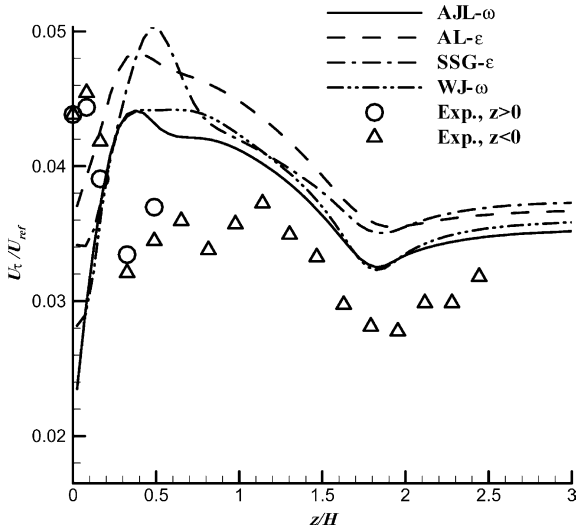

Fig. 14. 3-d Hill—distributions of friction velocity on lower wall at $x/H = 3.63$.

solutions, shown in Fig. 12 and characteristic of massive separation. In respect of model performance, Fig. 12 brings to light one interesting correspondence between the behaviour observed in the 2-d hill configuration and in the present flow, namely that the AJL model tends to give a relatively fast recovery from separation and the least excessive level of separation, while the WJ model returns the most exaggerated representation.

Consistent with the differences in mean flow, the computed turbulence energy, shown in Fig. 13, diminishes rapidly in the spanwise direction, confirming that the wake is confined to a much narrower region around the centre plane than its experimental counterpart.

The predicted skin-friction magnitude, shown in Fig. 14, is too low in the region $0 < z/H < 0.2$, but varies rapidly thereafter, again indicating an excessively narrow and intense wake with high momentum deficit. Beyond $z/H = 0.3$, the predicted value is too high, this region being mostly outside the computed wake, as is also recognised from the low predicted levels of turbulence energy at this spanwise location, Fig. 13.

Comparisons for the parameter S^{-1} have been included here, in Fig. 15, for the purpose of examining the near-wall behaviour of the stresses. The parameter does not, of course, provide information on the stresses

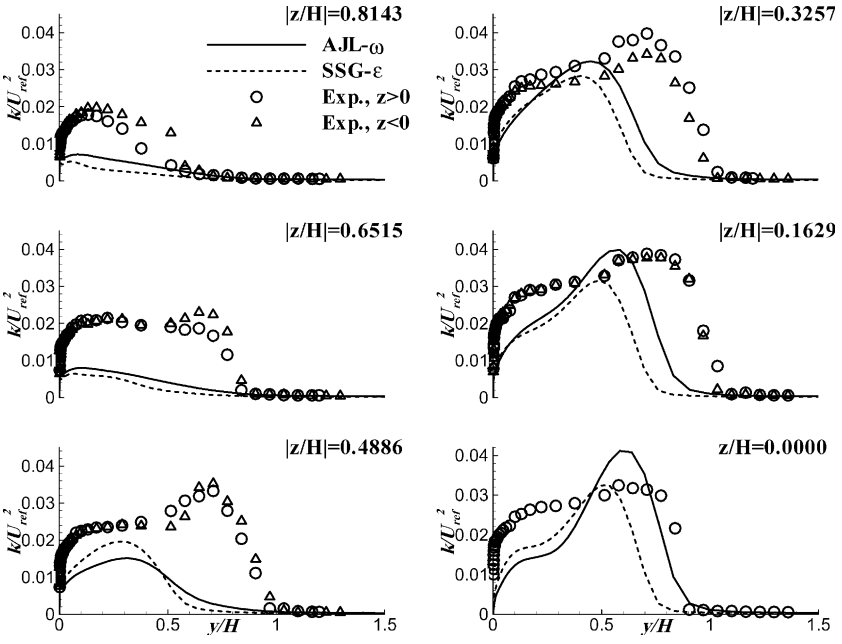

Fig. 13. 3-d Hill—profiles of turbulence energy at $x/H = 3.63$ and various spanwise z/H locations.

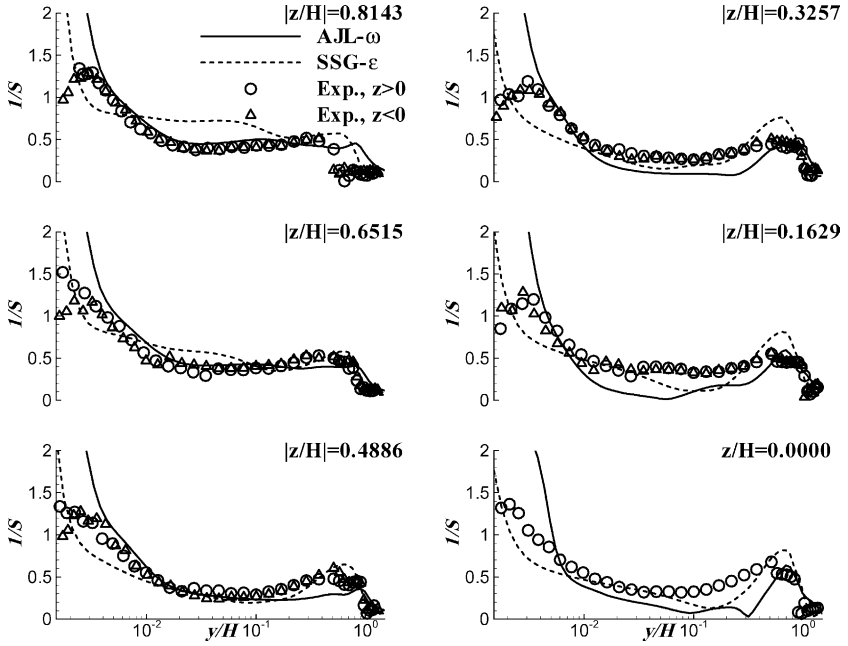

Fig. 15. 3-d Hill—profiles of $S^{-1} = \sqrt{(-\overline{uv})^2 + (-\overline{vw})^2}/\overline{vv}$ at $x/H = 3.63$ and various spanwise z/H locations.

themselves. These are unlikely to agree with the measurements, in view of the discrepancies observed in Figs. 9–14. It is recalled that the AJL model is designed to return the correct wall-asymptotic behaviour. This is indicated in Fig. 15, albeit qualitatively, by the sharp rise in S^{-1} as the wall is approached. This rise reflects the fact that the shear stresses decay (or should decay) at a rate $O(y^3)$, while the normal stress $\overline{v^2}$ should decay at the faster rate $O(y^4)$. The Reynolds-stress closure returns a qualitatively similar behaviour, but is not specifically formulated to give the correct wall-asymptotic decay of the stresses. The experimental data do not show the same rapid increase in this parameter, but their accuracy must be questionable very close to the wall.

The general behaviour observed above, especially in Figs. 11 and 12, is reminiscent of that returned by other RANS computations for bluff-body flow, in which large-scale, coherent, unsteady features associated with vortex shedding are not resolved, hence displaying excessive recirculation and insufficient rates of wake recovery and spread. In the light of this observation, some unsteady RANS computations have recently been performed with a second-order accurate scheme over the full channel width with the Apsley–Leschziner cubic eddy-viscosity model and the inlet flow perturbed periodically over a wide range of Strouhal numbers around a value of 0.2, based on hill height. In all circumstances, the unsteady solution returned to a steady state when the perturbation was removed. Large eddy simulations have also been performed for the present hill geometry, but at a Reynolds number of only 13,000, i.e. 10% of the experimental values, because of computer-resource limitations and the need to carefully resolve the near-wall region with a dense mesh. Time-averaged results have been compared to a steady-state calculation at the same Reynolds number performed with the Apsley–Leschziner model. The results of this study will be reported separately in Temmerman et al. (2004). Suffice it to report here that, at this much lower Reynolds number, the LES results suggest a much simpler separation behaviour than that shown in the experimentally-derived map included in Fig. 9. Correspondingly, agreement between the RANS computation and the simulation was found to be much closer. Hence, the LES computation does not, unfortunately, provide an explanation for the discrepancies recorded at $Re = 130,000$. To undertake credible, wall-resolved simulations at this high Reynolds number would be a major challenge and would in all likelihood require the use of a high-quality LES–RANS hybrid method.

5. Conclusions

A computational study has been undertaken to examine the ability of anisotropy-resolving turbulence models to predict 2-d and 3-d separation from curved surfaces forming hill-shaped obstructions. In the 2-d case, most models of this ilk over-estimate the size of the recirculation zone. This is associated with an insufficient level of the shear stress in the separated shear layer. An exception, in a number of respects, is the non-linear EVM model by Abe et al. (2003). This has been shown

here, as was done in an earlier study on a periodic segment, to give results quite close to the LES solution. The study has also demonstrated that the imposition of periodicity does not impact on the conclusions derived earlier: the present computations encompassing three hills with prescribed inlet conditions bring out the fact that a model performing poorly in periodic conditions performs (or at least may perform) even worse with prescribed inlet conditions.

Disappointingly, none of the models examined gives a satisfactory representation of the corresponding 3-d separation process, although there are not insignificant differences among the solutions. All computations appear to miss some important mechanisms that are responsible for the multiple-vortex structure in the wake. The predicted vortical separation encompasses a much too large portion of the leeward hill side, the reverse flow on this side is too intense, the wake is too narrow and its recovery too slow. Unsteady computations do not support the supposition that organised periodic motions associated with a shedding mechanism play a crucial role in causing the predictive errors. However, the inability of the models to represent the dynamics of large-scale eddies and unsteady separation can obviously not be ruled out. Nor do large eddy simulations, albeit at a much lower Reynolds number, provide indications on any specific mechanism that is missed. A resolution of this question may emerge from simulations at the correct Reynolds number, but these are bound to be extremely costly.

Acknowledgements

The authors are grateful to the UK Engineering and Physical Sciences Research Council, BAE Systems and the EU for their financial support of different parts of the research reported herein. The EU-funded work was undertaken within FLOMANIA (Flow Physics Modelling—An Integrated Approach), a collaboration between Alenia, AEA, Bombardier, Dassault, EADS-CASA, EADS-Military Aircraft, EDF, NUMECA, DLR, FOI, IMFT, ONERA, Chalmers University, Imperial College, TU Berlin, UMIST and St. Petersburg State University. The project is funded by the European Union and administrated by the CEC, Research Directorate-General, Growth Programme, under Contract No. G4RD-CT2001-00613.

References

Abe, K., Jang, Y.J., Leschziner, M.A., 2003. An investigation of wall-anisotropy expressions and length-scale equations for non-linear eddy-viscosity models. Int. J. Heat Fluid Flow 24, 181–198.

Apsley, D.D., Leschziner, M.A., 1998. A new low-Reynolds-number non-linear two- equation turbulence model for complex flows. Int. J. Heat Fluid Flow 19, 209–222.

Apsley, D.D., Leschziner, M.A., 1999. Advanced turbulence modelling of separated flow in a diffuser. Flow, Turbulence Combust. 63, 81–112.

Batten, P., Craft, T.J., Leschziner, M.A., Loyau, H., 1999. Reynolds-stress-transport modelling for compressible aerodynamics applications. J. AIAA 37, 785–797.

Chen, H.C., Jang, Y.J., Han, J.H, 2000. Computation of heat transfer in rotating two-pass square channels by a second-moment closure model. Int. J. Heat Mass Transfer 43, 1603–1616.

Craft, T.J., 1998. Developments in a low-Reynolds-number second-moment closure and its application to separating and reattachment flows. Int. J. Heat Fluid Flow 19, 541–548.

Craft, T.J., Launder, B.E., 1996. A Reynolds stress closure designed for complex geometries. Int. J. Heat Fluid Flow 17, 245–254.

Craft, T.J., Launder, B.E., Suga, K., 1996. Development and application of a cubic eddy-viscosity model of turbulence. Int. J. Heat Fluid Flow 17, 108–115.

Hanjalic, K., 1994. Advanced turbulence closure models: a view of current status and future prospects. Int. J. Heat Fluid Flow 15, 178–203.

Jakirlic, S., Hanjalic, K., 1995. A Second-moment closure for non-equilibrium and separating high- and low-Re-number flows. Proc. Tenth Symp. On Turbulent Shear Flows, Pennsylvania State University, pp. 23.25–23.30.

Jakirlic, S., Jester-Zuerker, R., Tropea, C. (Eds.), 2001. Proc. Ninth ERCOFTAC/IAHR/COST Workshop on Refined Turbulence Modelling, Darmstadt, October.

Jang, Y.J., Leschziner, M.A., Abe, K., Temmerman, L., 2002. Investigation of anisotropy- resolving turbulence models by reference to highly-resolved LES data for separated flows. Flow, Turbulence Combust. 69, 161–203.

Lien, F.S., Leschziner, M.A., 1994. A General non-orthogonal collocated finite volume algorithm for turbulent flow at all speeds incorporating second-moment turbulence-transport closure. Part I: Computational implementation. Comput. Methods Appl. Mech. Eng. 114, 123–148.

Lien, F.S., Leschziner, M.A., 1995. Modelling 2-d separation from high-lift aerofoils with a non-linear eddy-viscosity model and second-moment closure. The Aeronautical J. 99, 125–144.

Lien, F.S., Leschziner, M.A., 1997. Computational modelling of separated flow around streamlined body at high incidence. The Aeronautical J. 101, 269–275.

Manceau, R., Bonnet, J.-P. (Eds.), 2003. Proc. Tenth ERCOFTAC(SIG-15)/IAHR/QNET-CFD workshop on Refined Turbulence Modeling, October 10–11, 2002, University of Poitiers, France.

May, N.E., 1999. Intake/S-bend diffuser flow prediction using linear and non-linear eddy-viscosity and second-moment closure turbulence models. Eng. Turbulence Modell. Exp. 4, 329–338.

Rodi, W., Bonnin, J.-C., Buchal, P., Laurence, D. (Eds.), 1998. Testing of calculation methods for turbulent flows: workshop results for 5 test cases, EDF Report 98NB00004.

Simpson, R.L., Long, C.H., Byun, G., 2002. Study of vortical separation from an axisymmetric hill. Int. J. Heat Fluid Flow 23, 582–591.

Speziale, C.G., Sarkar, S., Gatski, T.B., 1991. Modelling the pressure-strain correlation of turbulence: an invariant dynamical systems approach. J. Fluid Mech. 227, 245–272.

Temmerman, L., Leschziner, M.A., Mellen, C., Frohlich, J., 2003. Investigation of wall-function approximations and subgrid-scale models in large eddy simulation of separated flow in a channel with streamwise periodic constrictions. Int. J. Heat Fluid Flow 24, 157–180.

Temmerman, L., Chen, W., Leschziner, M.A., 2004, A comparative study of separation from a three-dimensional hill using LES and

second-moment-closure RANS modeling. Submitted to Fouth European Congress on Computational Methods in Applied Sciences and Engineering, ECCOMAS 2004, Jyväskylä, Finland.

Wallin, S., Johansson, A.V., 2000. An explicit algebraic Reynolds stress model for incompressible and compressible turbulent flows. Journal of Fluid Mech 403, 89–132.